Materials & Design 236 (2023) 112468

Contents lists available at ScienceDirect

Materials & Design

journal homepage: www.elsevier.com/locate/matdes

Exploiting self-contact in mechanical metamaterials for new discrete functionalities

David Schwarz [a], Gerrit Felsch [a], Falk Tauber [a,b], Stefan Schiller [c], Viacheslav Slesarenko [a,*]

[a] Cluster of Excellence livMatS @ FIT – Freiburg Center for Interactive Materials and Bioinspired Technologies, Georges-Köhler-Allee 105, D-79110, Freiburg, Germany
[b] Plant Biomechanics Group (PBG) Freiburg @ Botanic Garden of the University of Freiburg, Freiburg, Germany
[c] Institute for Pharmaceutical Technology, Goethe University Frankfurt, Max-von-Laue-Str. 9, D-60438, Frankfurt, Germany

ARTICLE INFO

Keywords:
Metamaterials
Self-contact
Load-function systems
Logic
Tunability
Functionality

ABSTRACT

The rational geometric and topological organization of mechanical metamaterials allows for unconventional responses to external loads. These materials exhibit a coupling between deformation in orthogonal directions governed by Poisson's ratio, which, in turn, can be precisely adjusted through the deliberate selection of specific geometrical parameters within the metamaterial's structure. Although certain structural motifs may even enable a negative Poisson's ratio, it is conventionally assumed to remain constant or near-constant during deformation. In this study, we introduce a novel design concept that enables metamaterials to switch the sign of Poisson's ratio during loading, specifically at predetermined compressive strain levels, by harnessing self-contact between individual elements of the metamaterial. Through the integration of finite element simulations and experimental testing, we establish a direct correlation between the geometrical parameters of the unit cell and the mechanical response of the metamaterial. This correlation enables us to engineer samples with desired functionality and we present a discrete scales demonstrator that exploits this switchable behavior.

1. Introduction

The rational internal organization of mechanical metamaterials enables them to exhibit unconventional responses when subjected to mechanical loading. One of the most well-known manifestations of such unusual behavior can be observed in so-called auxetic materials [1]. Unlike conventional materials, which undergo lateral expansion when subjected to uniaxial compression, auxetic metamaterials exhibit simultaneous contraction in all directions, effectively exhibiting a negative Poisson's ratio [2]. Auxetic materials have garnered considerable attention as novel solutions for impact [3,4] or blast protection [5], sports equipment such as helmets [6] or shoes [7] and wearable electronics [8]. In biomedical applications, auxetic materials find utility in various areas [9], including coronary stents [10–12], bio-compatible porous implants [13–15], and scaffolds for tissue engineering [16–18]. The underlying internal organization responsible for the auxetic behavior has been replicated across multiple length scales, ranging from materials with nanoscale features [19,20], to materials with microscale dimensions [21], millimeter-sized features [22], and even structures spanning meters in one or two dimensions [23].

The global mechanical response of mechanical metamaterials is intrinsically linked to their internal periodic structure. Consequently, researchers primarily focus their attention on the design of the smallest building block - the unit cell [24]. Among auxetic metamaterials, one might distinguish several most common design motifs [1], such as honeycomb/reentrant cells [25,26], chiral patterns [27,28], and rotating rigid structures [29,30]. The reentrant unit cell, for example, consists of interconnected straight beams that fold inward upon compression, resulting in a negative Poisson's ratio. In this case, the Poisson's ratio value directly correlates with the geometrical characteristics of the unit cell, such as the length of the struts and the angle between them. The enduring popularity of the classical reentrant design stems from the clear deformation mechanism behind its negative Poisson's ratio [31]. Alternatively, for "intuitive" design, more direct methods can be employed in the search for new unit cells. For instance, Körner et al. [32] used eigenmode analysis to describe a family of lattices containing non-straight elements with auxetic behavior. Notably, a chiral lattice with sinusoidal curvy beam connections, as depicted in Fig. 1A, can exhibit auxetic behavior depending on the unit cell's geometry. Taking this concept further, Clausen et al. [33] utilized topology optimization to tune the Poisson's ratio of the lattice under tensile load, achieving

* Corresponding author.
E-mail address: viacheslav.slesarenko@livmats.uni-freiburg.de (V. Slesarenko).

https://doi.org/10.1016/j.matdes.2023.112468
Received 13 September 2023; Received in revised form 31 October 2023; Accepted 6 November 2023
Available online 13 November 2023

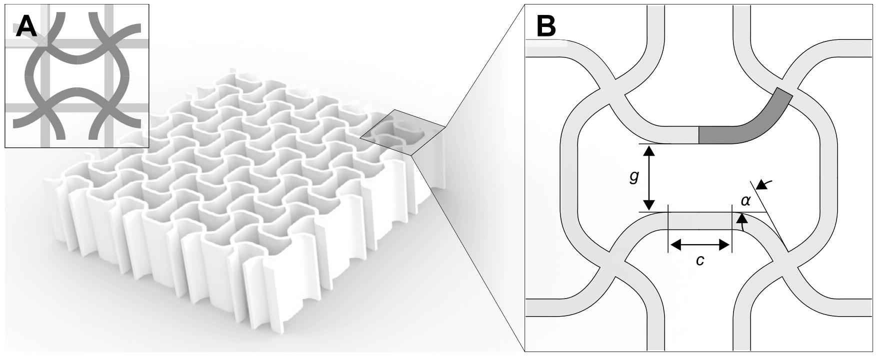

Fig. 1. Design of the unit cell and the resulting metamaterial. A: Base design is derived from a quadratic lattice (light grey), which is distorted to a sinusoidal lattice (dark grey) as described in [32]. B: Geometrical parameters g, and c defining the geometry of the unit cell.

values ranging from -0.8 to 0.8. It is worth noting that curved geometries have recently gained prominence for enriching the design space and expanding the range of admissible properties in mechanical metamaterials [34–36].

It has been observed that contact between the elements of metamaterials can occur under sufficiently large compressive strain [37]. Consequently, the response of the metamaterial suddenly becomes much stiffer as compared with the initial stage of compression [38]. Therefore, depending on the applied deformation, such a lattice may exhibit two distinctly different behaviors, effectively switching between them. In general, the ability to control the behavior of metamaterials by manipulating their internal architecture after fabrication is highly desirable. To achieve this, both mechanical and non-mechanical external stimuli can be harnessed. For instance, non-mechanical control through temperature changes has shown the potential to alter the Poisson's ratio of metamaterials containing active materials such as hydrogels [39], shape memory polymers [40], or liquid crystal elastomers [41]. The employment of magnetic interaction between the metamaterial's components enables another avenue for tuning their behavior [42–44]. Additionally, more exotic next-generation smart materials, capable of adapting and learning [45–47], might enable the attainment of more intelligent control over architectural changes in metamaterials, thus expanding their application scope. For already reported metamaterials, control via mechanical stimuli relies on intricate coupling between various loading sequences [48], instability-driven transformations [49,50], or self-contact between elements [51]. The latter approach relies solely on the internal geometry and, due to its relative simplicity, can open new avenues for introducing novel functionalities in metamaterials that emerge from changes in behavior during deformation. For example, the implementation of contact between unit cells has enabled the realization of 'if-then-else' functionality [52]. Similarly, alternating Poisson's ratios under load have been achieved through sequentially activated self-contacts [53] or sliding and locking mechanisms [54]. Helou et al. [55] utilized self-contact in a classical rotating-square design to embed electrical circuits that can close upon self-contact, demonstrating basic computational capabilities stemming from the rational architecture of metamaterials. These mechanisms for smart property switching are part of the emerging field of mechanical computing [56].

Self-contact presents a unique opportunity to facilitate functionalities based on discrete states and to achieve transitions resulting from abrupt changes in mechanical responses. In this context, the previously mentioned sinusoidal lattice [33,34,37] exhibits intriguing properties: when subjected to compression, we observe alterations in lattice connectivity due to self-contact, which can be harnessed to influence the resulting Poisson's ratio. In this study, we systematically evaluate the contact-induced changes in mechanical response concerning the unit cell's geometry. Furthermore, we apply these metamaterials in the design of scales-like devices, capitalizing on the anticipated auxeticity switches.

2. Unit cell and design space

2.1. Shape definition

Fig. 1 presents the mechanical metamaterial based on curvy connections. For parameterized scripting of the unit cell, we utilized the Grasshopper module of Rhino 7 (Robert McNeel & Associates, Seattle, USA). The unit cell of the metamaterial under consideration is uniquely defined by the shape of a single beam. By employing circular patterning around its bent end, followed by horizontal and vertical mirroring, we derived the unit cell depicted in Fig. 1B. We achieved a diverse range of unit cell geometries by manipulating two key geometric parameters: gap size (g) and contact length (c). It is worth noting that the angle α, as shown in Fig. 1B, is exclusively determined by g and c, both expressed as percentages of the unit cell's width/height. Additionally, we maintained a consistent beam cross-section by setting the curvy beams' widths to 5% of the unit cell's size.

2.2. Shape changes

We demonstrate the parameter space of the considered designs (Fig. 2), alongside two examples of the "most extreme" unit cells. This two-dimensional design space was probed in 15 equidistant steps per parameter. The range of values for contact length (c) spanned from 1% to 50% of the unit cell size, while gap sizes (g) ranged from 1% to 15%. The boundaries for the gap size were established to prevent initial contact at minimum value and ensure gap closure at a reasonable compression level when set to $g = 15\%$. This approach effectively captures the influence of gap size g and contact length c on the angle α and ensures the overall continuity of the parameter space, as depicted in Fig. 2.

3. Simulations for characterization

3.1. Simulation setup

With sufficient coverage of the parameter space, we conducted a detailed investigation into the mechanical behavior of selected metamaterials under compression using finite element (FE) analysis. This analysis was performed using COMSOL Multiphysics 6.0 (Comsol AB, Stockholm, Sweden), with a specific focus on studying the changes in properties induced by self-contact. Prior to importing the 2D representations of the unit cells, we applied a 25% shift in both the vertical and horizontal directions. This adjustment was made to ensure more reliable meshing and simplify the imposition of periodic boundary conditions. Additionally, we filleted sharp corners to prevent singularities during simulations. Each geometry was meshed with a minimum of five second-order quad elements spanning the width of the curvy beam structures.

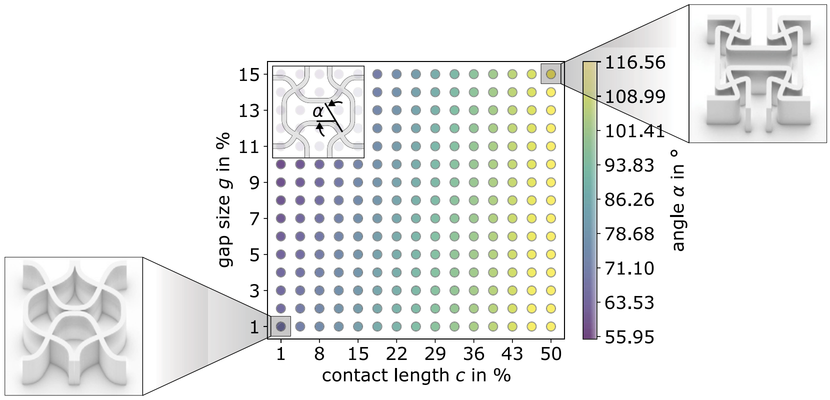

Fig. 2. Parameter space (g and c) coverage with angle α shown in color. Two extreme examples of the unit cells are shown in the corners.

We selected an incompressible neo-Hookean material model, with a Lamé parameter (μ) set to 2.93 MPa, to closely match the properties of the 3D-printable NinjaFlex thermoplastic polyurethane (TPU) filament, as reported in [57]. Furthermore, in Section 4, we employed experimental testing to assess the adequacy of this material model. To accurately capture the mechanical response of the unit cell, including self-contact, we incorporated geometric non-linearity and allowed contact between all boundaries. The application of strain and periodicity to the lattice was facilitated by a set of periodic boundary conditions.

$$v(T) - v(B) = -\varepsilon_y \cdot l_0 \tag{1}$$

$$u(T) - u(B) = 0 \tag{2}$$

$$v(L) - v(R) = 0 \tag{3}$$

$$u(L) - u(R) = u(p_1) - u(p_2), \tag{4}$$

with T, B, L and R being the top, bottom, left and right boundaries, respectively, and l_0 being the initial height of the unit cell. Here v and u are displacements in x and y direction. Note that further we assume that the height and width of the unit cell to be equal to 1 initially. In the boundary condition (1), we apply a compression strain ε_y. The maximum applied strain was set to $3.5g$ or 25% of the initial height, whichever was lower (see Fig. 3). This limit was chosen to ensure the convergence of the simulation by preventing extremely large deformations after self-contact was reached. By analyzing the evolution of the coordinates of two corner points, we obtained the engineering and instantaneous Poisson's ratios ν_{eng} and ν_{inst} of the lattice, as defined by [58]:

$$\nu_{eng} = -\frac{\varepsilon_x}{\varepsilon_y} \tag{5}$$

$$\nu_{inst} = -\frac{\varepsilon_{inst,x}}{\varepsilon_{inst,y}} \tag{6}$$

Here, ν_{eng} reflects the deformation of the metamaterial in relation to the initial undeformed configuration. For instance, if $\nu_{eng} < 0$, then it is guaranteed that the current width of the metamaterial under compression is smaller than the original one. In contrast, ν_{inst} compares current strains to strains at the previous moment in time. Therefore, it might occur that ν_{eng} is still negative while the metamaterial is in the process of expansion characterized by $\nu_{inst} > 0$. To be precise, each Poisson's definition relies on a differently defined strain ε_{eng} and ε_{inst}. Strains $\varepsilon_{eng,j}$ were calculated from the point coordinates, as depicted in Fig. 3. Specifically, they were calculated with respect to initial dimension values $l_{0,j}$, with $j = x, y$:

$$\varepsilon_{eng,j} = \frac{l_{i,j} - l_{0,j}}{l_{0,j}} \tag{7}$$

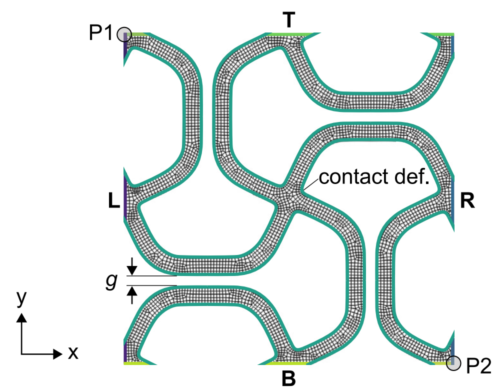

Fig. 3. Meshed lattice with evaluation points and contact definition boundaries shown in green.

For ε_{inst}, we used previous dimension values $l_{i-1,j}$:

$$\varepsilon_{inst,j} = \frac{l_{i,j} - l_{i-1,j}}{l_{i-1,j}} \tag{8}$$

$l_{i,j}$ being the current distance between the corner points p_1 and p_2 in x- and y-directions for $\varepsilon_{inst,x}$ and $\varepsilon_{inst,y}$, respectively.

3.2. Results and discussion

In Fig. 4, we present a typical response of the unit cell, which can be divided into three distinctive zones or regimes (I-III) with two transition points (P_S and P_E) that can be evaluated for each unit cell. In the initial phase of compressive loading, we observe auxetic behavior (regime I), characterized by a negative Poisson's ratio (both ν_{inst} and ν_{eng}). Subsequently, self-contact occurs at point P_S ($\varepsilon = \varepsilon^{cont}$), leading to a change in topology. This change results in a significant jump in the instantaneous Poisson's ratio (ν_{inst}), followed by a gradual increase in the value of the engineering Poisson's ratio (ν_{eng}) in regime II. As compression continues, the lattice may reach its initial width at point P_E, coinciding with $\nu_{eng} = 0$. Finally, the lattice continues to expand beyond its initial width, maintaining positive values for both ν_{eng} and ν_{inst} in regime III.

A similar observation can be made regarding the evolution of the metamaterial's stiffness during compression. Upon self-contact, the metamaterial undergoes a noticeable stiffening, which is visible on the stress-strain curve (Fig. 4B). In a similar fashion to ν_{inst}, the instantaneous Young's modulus E_{inst}, defined as the slope of the stress-strain curve at each specific point, exhibits a step-like jump upon contact (Fig. 4B). The difference in stiffness (E_{inst}) before and after self-contact can be attributed to the underlying deformation mechanisms. Prior to contact, deformation is mostly facilitated via the rotation in the lattice's

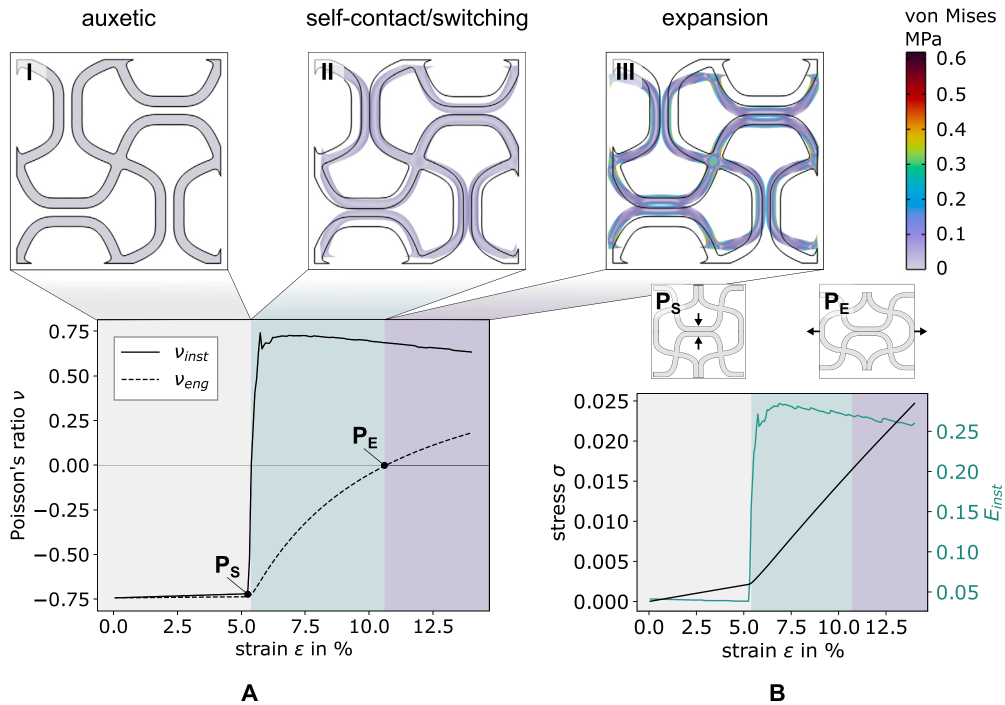

Fig. 4. Typical response of the metamaterial during compression. A: Poisson's ratio I: Auxetic behavior is seen ($\nu_{inst} < 0$ and $\nu_{eng} < 0$). II: After self-contact at strain ε^{cont} (point P_S), switching of instantaneous Poisson's ratio sign can be observed ($\nu_{inst} > 0$ and $\nu_{eng} < 0$). III: Expansion beyond initial width after reaching ε^{exp} (point P_E) corresponding to the case of $\nu_{inst} > 0$ and $\nu_{eng} > 0$. B: Stress σ and E_{inst} during compression.

nodes. However, this rotational motion becomes constrained upon self-contact, resulting in a deformation dominated by bending of the beams in regimes II and III (Fig. 4 and supplementary video 1). It is worth noting that stiffening of the metamaterial also leads to an increase in the level of internal stresses. The maximal stresses are usually observed in the lattice nodes and in contact zones; however, due to the length of such zones, there is no pronounced stress concentration after self-contact that might lead to crack initiation.

The strain at which self-contact occurs (ε^{cont}) is depicted for each geometry from the considered parameter space in Fig. 5A. Here we can observe the anticipated relation between ε^{cont} and g. Indeed, specimens with larger initial gap g require larger strain before self-contact takes place. Specifically, ε^{cont} spans from 1% to 21% for the minimum and maximum gap sizes g, respectively. In contrast, we observe a minimal influence of the contact length (c) on the strain ε^{cont} required for self-contact. This indifference can be attributed to the fact that during the initial stages of compression, deformation primarily occurs due to bending and rotation near the intersection nodes, while straight elements do not significantly contribute to ν_{inst} in stage I. However, the contact length (c) plays a crucial role in determining the height of the jump in the value of ν_{inst} upon reaching ε^{cont}.

While for all considered geometries ν_{inst} increases after self-contact, in some cases it does not reach 0 and continues to be negative. This behavior is typical for lattices with large contact lengths ($c > 40\%$), as indicated by the points marked with a cross in Fig. 5A. Consequently, these metamaterials do not undergo a switch in the sign of the instantaneous Poisson's ratio (ν_{inst}) and maintain their auxetic behavior after self-contact. The consequence of this behavior is an inability to return to the original width, as the lattice continues to shrink laterally during subsequent compression.

The distinction between designs that switch or don't switch their auxeticity due to self-contact visible in Fig. 5A can assist in selecting unit cells tailored for a specific use-case. For instance, if maintaining the auxeticity after self-contact is favorable for impact engineering, the lattices with large enough c are well-suited according to this criterion. These designs offer the dual benefit of maintaining auxeticity and the ability to significantly stiffen the material upon reaching a pre-programmed deformation level [38]. At the same time, the switch in the sign of instantaneous Poisson's ratio can be harnessed for novel use-cases, such as mechanical if-then switches activated upon achieving specific compressive strains. Since self-contact in such lattices only facilitates a change in the sign of ν_{inst} rather than ν_{eng}, it becomes essential to determine the strain value ε^{exp} at which the metamaterial expands beyond its initial width. Fig. 5B utilizes color coding to indicate the values of ε^{exp}. For points in the parameter space marked by a cross, no expansion occurs because the corresponding unit cells do not undergo a switch in auxeticity. For points marked by empty circles, expansion occurs; however, after reaching 25% compressive strain, the lattice's width is still smaller than the initial width. From a practical standpoint, we limit our focus to lattices that expand beyond their initial width at compressive strains less than 25%. This mapping of ε^{exp} onto the geometrical parameters defining unit cell design allows for the deliberate selection of geometries with specific sequences of lateral shrinking and expansion during compression. Since expansion occurs at larger values of strain than self-contact, we additionally utilize experimental testing to ensure accuracy of our model.

4. Experimental testing

4.1. Experimental setup

To confirm the observed non-trivial behavior and validate the obtained dependencies, we conducted compressive experiments on 3D-printed specimens. We carefully selected 10 different unit cell designs to ensure maximum representation of the parameter space, as illustrated in Fig. 6. These lattice specimens were fabricated using fused filament fabrication (FFF) with NinjaFlex TPU (NinjaTek, Lititz, USA). The specimens were composed of 20 mm unit cells arranged in a 3 × 3 pattern. We performed compression testing on a uniaxial testing machine (ZwickRoell, Ulm, Germany) equipped with a 10 kN loadcell. The load cycle was comprised of 15 mm vertical compression with subsequent unloading at a constant testing speed of 15 mm min^{-1}. Note that

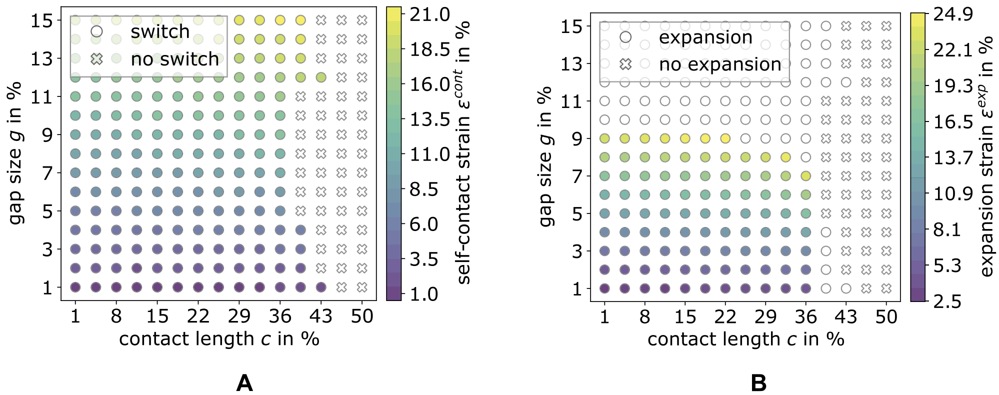

Fig. 5. A: Value of the self-contact strain ε^{cont} for different unit cells in the design space. Combinations marked by cross do not exhibit switch in the sign of the Poisson's ratio. B: Strain at the onset of expansion beyond the initial width ε^{exp} for different geometrical parameters c and g. Empty circles mark combinations of geometrical parameters for which the expansion happens for strains exceeding 25%. Cross sign marks geometrical parameters for which $\nu_{inst} < 0$ even after self-contact.

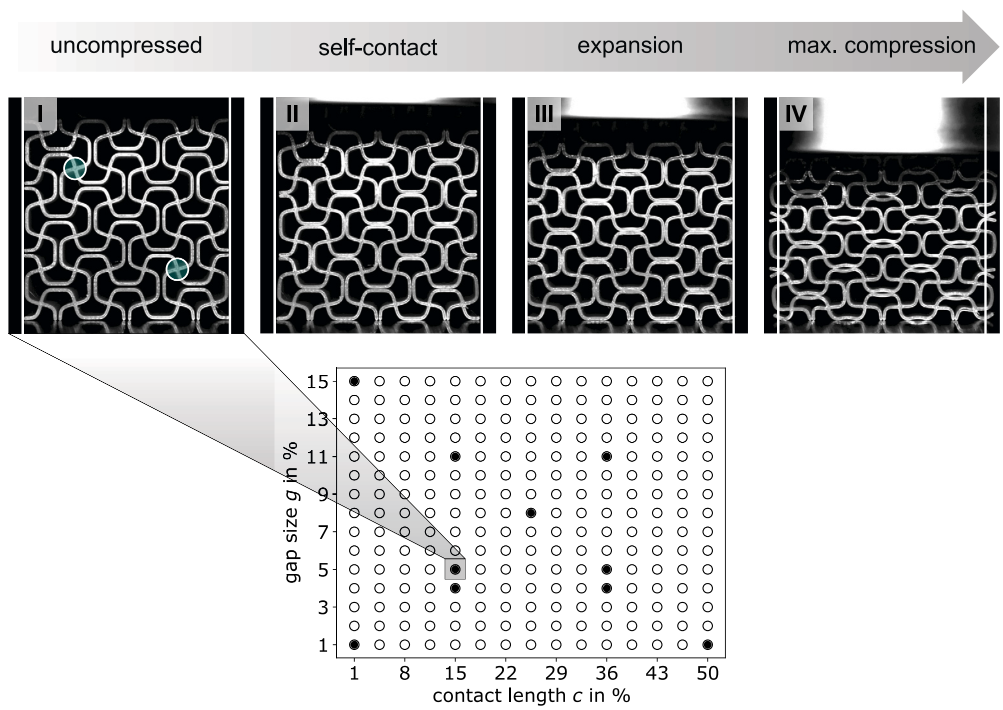

Fig. 6. Experimentally tested specimens are depicted as filled circles in the parameter space. The evolution of specimen shape throughout compression. I: uncompressed state ($\varepsilon = 0$), II: self-contact ($\varepsilon = \varepsilon^{cont}$), III: start of the expansion beyond initial width ($\varepsilon = \varepsilon^{exp}$), IV: maximum compression ($\varepsilon = 25\%$). Vertical lines indicate the initial width of 60 mm, tracked points are shown as filled circles in I.

15 mm vertical displacement on the considered specimens corresponds precisely to 25% strain. We used video recordings for characterization of the lattice's deformation under load. The positions of two points on the lattice (indicated by circles in Fig. 6) were automatically tracked to retrieve two values of interest: the strain of self-contact (ε^{cont}) and, if observable, the strain of expansion beyond initial width ε^{exp}.

Fig. 6I-IV provides a visual representation of the status of the tested specimen at various compression levels. The act of compressing the specimen results in the closure of the initial gap, introducing self-contact in predefined areas, as shown in Fig. 6II. Additionally, we observe lateral shrinkage of the specimen concerning the lines that indicate the initial width. This observation is indicative of the specimen's auxetic behavior before self-contact occurs. Upon self-contact that happens nearly simultaneously between all contact zones, the shrinking process halts, and the specimen begins to undergo lateral expansion. This expansion is evident as the specimen touches the white lines representing the initial width in Fig. 6III. Furthermore, it expands beyond these lines with an increase in applied compressive strain, as demonstrated in Fig. 6IV (for specimen compression, see supplementary video 1).

4.2. Validation and characterization

Qualitatively, we have confirmed the behavior previously observed in simulations, and we have identified the distinct phases of mechanical response, as depicted in Fig. 4. The validation of self-contact and expansion values for all tested specimens empowers us to harness these mechanical response phases for practical applications. For all 10 tested specimens, we extracted values of ε^{cont} and ε^{exp} where possible. When comparing experimentally obtained self-contact strain ε^{cont} with numerically predicted values, we find a substantial agreement with an R^2 value of 0.9401 (Fig. 7A). As applied strain increases, lattices with shorter contact lengths (c) undergo an auxeticity-switch. Consequently,

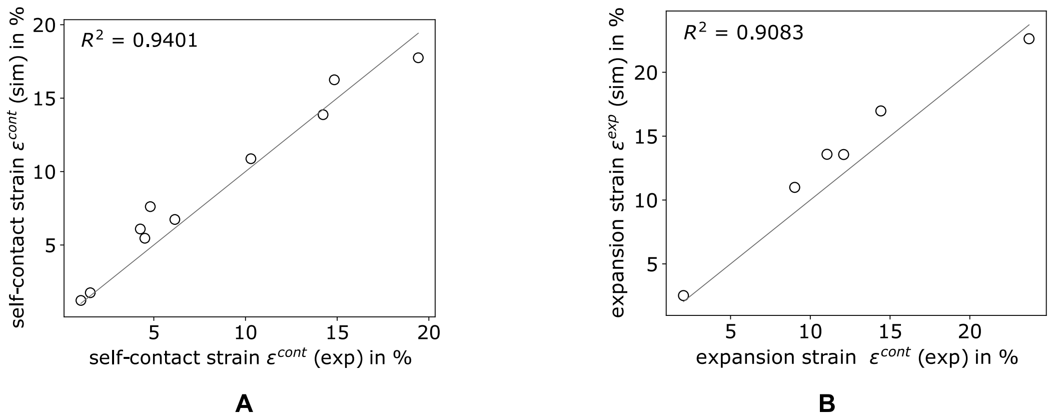

Fig. 7. Simulations vs experiments. A: Strain at observed self-contact ε^{cont}. B: Onset of expansion beyond the initial width ε^{exp}.

we compared numerically predicted and experimentally obtained expansion strains (ε^{exp}) for such lattices, as shown in Fig. 7B. Despite the need to exclude lattices that either do not expand at all or don't exhibit expansion beyond the initial width for applied strains less than 25%, we observe a strong agreement between experiments and simulations, with an R^2 value of 0.9083. It is worth noting that numerical simulations generally slightly overestimate strains associated with self-contact and expansion beyond the initial width as compared with experiments. This minor discrepancy may be attributed to geometric imperfections introduced by the 3D printing process. Specifically, the gap size in the printed samples might be smaller than designed due to finite value of extrusion width that cannot be arbitrary low, resulting in slightly thicker printed beams.

In summary, our performed numerical simulations not only capture the real auxeticity switch induced by self-contact in the considered metamaterials but also provide us with reliable estimates of the specific strain levels at which contact or expansion beyond the original boundaries occurs.

5. Scales demonstrator

To demonstrate the applicability of the introduced design framework, we developed a discrete scales demonstrator that relies on the switches in Poisson's ratio caused by self-contact in the metamaterial. We created four specimens with identical outer dimensions (as used in Section 4) but with different geometrical parameters (c and g). These specimens were 3D-printed using conductive Filaflex TPU filament (Recreus, Elda, Spain). Utilizing the information from Fig. 5B, we selected specimens with varying expansion strains (ε_i^{exp}), where $i = 1 \dots 4$. These strains amounted to $5.2\%, 13\%, 20.9\%$ and $>25\%$ respectively. The 3D-printed specimens were placed within an enclosure, as illustrated in Fig. 8A. In their undeformed state, each specimen made contact with corresponding electrodes integrated into the enclosure, which were connected to pairs of LEDs, as depicted in Fig. 8B. These LEDs were placed behind their corresponding specimens to illuminate them upon reaching pre-programmed strains that results in closure of the electric circuit. To ensure even load distribution during compression, we covered the assembled system with a lid. Subsequently, the system was positioned in a universal testing machine, with two perpendicular mirrors placed behind it to facilitate video capturing of three sides of the scale demonstrator.

In the initial uncompressed state, all metamaterials are illuminated from inside the scales, as shown in Fig. 8C. Almost immediately after the compression begins, the lattices lose contact with the electrodes due to their auxetic behavior, which facilitates lateral shrinking, resulting in all LEDs switching off. As compression continues, the LEDs gradually light up the connected lattices one by one. The side of the cube containing the metamaterial with the lowest expansion strain (ε_1^{exp}) is the first to illuminate. In a cascading manner, the specimens light up as their specified expansion strains (ε_i^{exp}) are reached. During unloading, the illumination on the sides of the specimens switches off in the opposite sequence until all LEDs are off when the applied strain drops below ε_1^{exp}. In addition, at the latest stage of unloading, when the metamaterials return to their initial undeformed state, all sides of the scales demonstrator are illuminated again, indicating that the scales are "self-calibrated" and ready for the next measurement. This behavior is proven to be repeatable during multiple consecutive loading-unloading cycles for applied strains less than 25% (for a scales demonstration, see supplementary video 2).

Since values of ε_i^{exp} are known and, moreover, purposefully selected, LED states enable us to deduct the applied strain, or at the least, place it within a specific range. If all LEDs are off, it indicates that the applied strain is lower than ε_1^{exp}. If only two LEDs are on, it suggests that the applied strain falls within the range between ε_2^{exp} and ε_3^{exp}. Moreover, this concept can be repurposed for measuring force instead of strain. Within the proposed design, the reaction force monotonically increases with an increase in applied compressive strain, as observed in load-cell data. This is because there are no snap-through transitions within the metamaterial. Consequently, a correspondence between force and strain, and thus between force and LED states, can be established. Additionally, within this concept, we can even detect faults in the electric circuitry. For example, if one of the LEDs fails to illuminate after complete unloading, it may indicate a faulty contact.

This approach can therefore be implemented for targeted applications of the presented lattice. Here, not only the expansion but also the sudden change of the sign of Poisson's ratio upon self-contact can be considered as a feature, with results from Fig. 5 serving as a lookup table to further enhance the utility of metamaterial.

6. Conclusion

In this study, we explored the concept of mechanical metamaterials capable of switching their Poisson's ratio at a pre-programmed strain level (ε^{cont}) by harnessing self-contact between metamaterial elements. For a selected design inspired by metamaterials with curvy beams, we assessed the relationship between the geometrical characteristics of unit cells and the resulting mechanical response through simulations and experimental testing. In the continuous design space, we identified geometry parameters that result in different shrinking-expansion sequences. We demonstrated, that for specific unit cells, self-contact immediately changes the instantaneous Poisson's ratio, but the metamaterial continues to shrink laterally upon subsequent compression. Meanwhile, for another class of unit cells, self-contact facilitates a change in the effective Poisson's ratio sign, leading to the expansion of the metamaterial and eventual expansion beyond its initial dimensions for larger compressive strain (ε^{exp}). We showed how these critical strains (ε^{cont} and

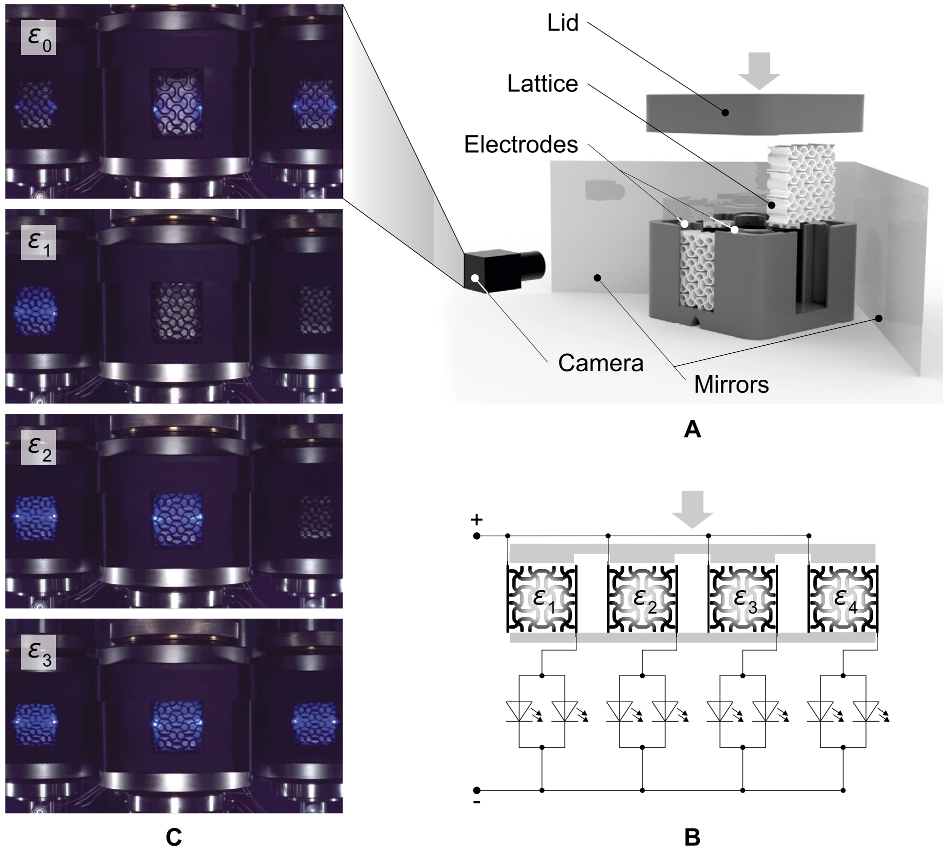

Fig. 8. Discrete scales demonstrator. A: Components of the demonstrator. B: Circuitry of the demonstrator containing two LEDs per lattice with pre-programmed expansion strain ε^{exp}_{1-4}. C: Scales during compression testing, mirrors allow observation of three sides at once. Initially all circuits are closed at $\varepsilon_0 = 0$. Subsequently, all LEDs switch off until the lattices close their circuits at individual expansion strains ε^{exp}_i.

ε^{exp}) can be tuned via the geometry of the unit cell to enable novel functionalities in the corresponding metamaterials. Utilizing numerical and experimental results, we created a demonstrator model of a discrete scales-like device capable of indicating the applied strain through the statuses of multiple LEDs. During compression, the sides of the demonstrator light up one by one upon reaching the selected critical strains, triggered by switches in the Poisson's ratio caused by self-contact. It is important to note that in this proposed concept the self-contact functionality is integral part of the metamaterial's load-bearing core, which significantly simplifies the design. The findings presented here can be applied to implement the lattice's switching capabilities in complex applications, such as soft robotics or lifelike stimuli-responsive material systems.

Declaration of competing interest

The authors declare that they have no known competing financial interests or personal relationships that could have appeared to influence the work reported in this paper.

Data availability

Data will be made available on request.

Acknowledgement

Funded by the Deutsche Forschungsgemeinschaft (DFG, German Research Foundation) under Germany's Excellence Strategy – EXC-2193/1 – 390951807. S. Schiller gratefully acknowledges the 'Alfons und Gertrud Kassel-Stiftung, Frankfurt am Main'. The authors acknowledge support by the state of Baden-Württemberg through bwHPC and the German Research Foundation (DFG) through grant no INST 39/963-1 FUGG (bwForCluster NEMO). The authors acknowledge support by the Open Access Publication Fund of the University of Freiburg.

Appendix A. Supplementary material

Supplementary material related to this article can be found online at https://doi.org/10.1016/j.matdes.2023.112468.

References

[1] H.M.A. Kolken, A.A. Zadpoor, Auxetic mechanical metamaterials, RSC Adv. 7 (9) (2017) 5111–5129.
[2] X. Ren, R. Das, P. Tran, T.D. Ngo, Y.M. Xie, Auxetic metamaterials and structures: a review, Smart Mater. Struct. 27 (2) (2018) 023001.
[3] F. Usta, H.S. Türkmen, F. Scarpa, Low-velocity impact resistance of composite sandwich panels with various types of auxetic and non-auxetic core structures, Thin-Walled Struct. 163 (2021) 107738.
[4] A. Bührig-Polaczek, C. Fleck, T. Speck, P. Schüler, S.F. Fischer, M. Caliaro, M. Thielen, Biomimetic cellular metals—using hierarchical structuring for energy absorption, Bioinspir. Biomim. 11 (4) (2016) 045002.
[5] R.P. Bohara, S. Linforth, T. Nguyen, A. Ghazlan, T. Ngo, Anti-blast and -impact performances of auxetic structures: a review of structures, materials, methods, and fabrications, Eng. Struct. 276 (2023) 115377.
[6] O. Duncan, T. Shepherd, C. Moroney, L. Foster, P. Venkatraman, K. Winwood, T. Allen, A. Alderson, Review of auxetic materials for sports applications: expanding options in comfort and protection, Appl. Sci. 8 (6) (2018) 941.
[7] A. Papadopoulou, J. Laucks, S. Tibbits, Auxetic materials in design and architecture, Nat. Rev. Mater. 2 (12) (2017).
[8] S. Han, E.J. Lee, B. Kim, S. Jung, S. Jeong, S.-W. Kim, Y. Choi, S.Y. Lee, High-performance dual-mode triboelectric nanogenerator based on hierarchical auxetic structure, ACS Energy Lett. 5 (11) (2020) 3507–3513.
[9] S. Shukla, B.K. Behera, Auxetic fibrous materials and structures in medical engineering – a review, J. Text. Inst. 114 (7) (2022) 1078–1089.

[10] F. Amin, M.N. Ali, U. Ansari, M. Mir, M.A. Minhas, W. Shahid, Auxetic coronary stent endoprosthesis: fabrication and structural analysis, J. Appl. Biomater. Funct. Mater. 13 (2) (2015) 127–135.
[11] R. Gatt, L. Mizzi, J.I. Azzopardi, K.M. Azzopardi, D. Attard, A. Casha, J. Briffa, J.N. Grima, Hierarchical auxetic mechanical metamaterials, Sci. Rep. 5 (1) (2015).
[12] H. Jiang, H. Ziegler, Z. Zhang, H. Zhang, L.L. Barbenchon, S. Atre, Y. Chen, 3d printed tubular lattice metamaterials for mechanically robust stents, Composites, Part B, Eng. 236 (2022) 109809.
[13] H.M.A. Kolken, S. Janbaz, S.M.A. Leeflang, K. Lietaert, H.H. Weinans, A.A. Zadpoor, Rationally designed meta-implants: a combination of auxetic and conventional meta-biomaterials, Mater. Horiz. 5 (1) (2018) 28–35.
[14] N. Ghavidelnia, M. Bodaghi, R. Hedayati, Femur auxetic meta-implants with tuned micromotion distribution, Materials 14 (1) (2020) 114.
[15] A. Sharipova, I. Gotman, S. Psakhie, E. Gutmanas, Biodegradable nanocomposite Fe–Ag load-bearing scaffolds for bone healing, J. Mech. Behav. Biomed. Mater. 98 (2019) 246–254.
[16] Y. Jin, C. Xie, Q. Gao, X. Zhou, G. Li, J. Du, Y. He, Fabrication of multi-scale and tunable auxetic scaffolds for tissue engineering, Mater. Des. 197 (2021) 109277.
[17] G. Flamourakis, I. Spanos, Z. Vangelatos, P. Manganas, L. Papadimitriou, C. Grigoropoulos, A. Ranella, M. Farsari, Laser-made 3d auxetic metamaterial scaffolds for tissue engineering applications, Macromol. Mater. Eng. 305 (7) (2020).
[18] Ó. Lecina-Tejero, M.Á. Pérez, E. García-Gareta, C. Borau, The rise of mechanical metamaterials: auxetic constructs for skin wound healing, J. Tissue Eng. 14 (2023).
[19] L. Mizzi, E. Salvati, A. Spaggiari, J.-C. Tan, A.M. Korsunsky, 2d auxetic metamaterials with tuneable micro-/nanoscale apertures, Appl. Mater. Today 20 (2020) 100780.
[20] J. Valente, E. Plum, I.J. Youngs, N.I. Zheludev, Nano- and micro-auxetic plasmonic materials, Adv. Mater. 28 (26) (2016) 5176–5180.
[21] K.K. Dudek, J.A.I. Martínez, G. Ulliac, M. Kadic, Micro-scale auxetic hierarchical mechanical metamaterials for shape morphing, Adv. Mater. 34 (14) (2022).
[22] L.Y.W. Loh, U. Gupta, Y. Wang, C.C. Foo, J. Zhu, W.F. Lu, 3d printed metamaterial capacitive sensing array for universal jamming gripper and human joint wearables, Adv. Eng. Mater. 23 (5) (2021).
[23] R.P. Bohara, S. Linforth, T. Nguyen, A. Ghazlan, T. Ngo, Dual-mechanism auxetic-core protective sandwich structure under blast loading, Compos. Struct. 299 (2022) 116088.
[24] X. Yu, J. Zhou, H. Liang, Z. Jiang, L. Wu, Mechanical metamaterials associated with stiffness, rigidity and compressibility: a brief review, Prog. Mater. Sci. 94 (2018) 114–173.
[25] U. Larsen, O. Signund, S. Bouwsta, Design and fabrication of compliant micromechanisms and structures with negative Poisson's ratio, J. Microelectromech. Syst. 6 (2) (1997) 99–106.
[26] Z. Chen, X. Wu, Y.M. Xie, Z. Wang, S. Zhou, Re-entrant auxetic lattices with enhanced stiffness: a numerical study, Int. J. Mech. Sci. 178 (2020) 105619.
[27] D. Mousanezhad, B. Haghpanah, R. Ghosh, A.M. Hamouda, H. Nayeb-Hashemi, A. Vaziri, Elastic properties of chiral, anti-chiral, and hierarchical honeycombs: a simple energy-based approach, Theor. Appl. Mech. Lett. 6 (2) (2016) 81–96.
[28] K.K. Dudek, New type of rotation of chiral mechanical metamaterials, Smart Mater. Struct. 29 (11) (2020) 115027.
[29] J.N. Grima, K.E. Evans, Auxetic behavior from rotating squares, J. Mater. Sci. Lett. 19 (17) (2000) 1563–1565.
[30] V. Slesarenko, Planar mechanical metamaterials with embedded permanent magnets, Materials 13 (6) (2020) 1313.
[31] R.F. Almgren, An isotropic three-dimensional structure with Poisson's ratio =-1, J. Elast. 15 (4) (1985) 427–430.
[32] C. Körner, Y. Liebold-Ribeiro, A systematic approach to identify cellular auxetic materials, Smart Mater. Struct. 24 (2) (2014) 025013.
[33] A. Clausen, F. Wang, J.S. Jensen, O. Sigmund, J.A. Lewis, Topology optimized architectures with programmable Poisson's ratio over large deformations, Adv. Mater. 27 (37) (2015) 5523–5527.
[34] J.C. McCaw, E. Cuan-Urquizo, Curved-layered additive manufacturing of non-planar, parametric lattice structures, Mater. Des. 160 (2018) 949–963.
[35] G. Felsch, N. Ghavidelnia, D. Schwarz, V. Slesarenko, Controlling auxeticity in curved-beam metamaterials via a deep generative model, Comput. Methods Appl. Mech. Eng. 410 (2023) 116032.
[36] V. Slesarenko, Bandgap structure in elastic metamaterials with curvy Bezier beams, Appl. Phys. Lett. 123 (8) (2023).
[37] J. Dong, G. Ye, Y. Wang, F. Jin, H. Fan, Design, manufacture and crushing behaviors of buckling-inspired auxetic meta-lattice structures, Int. J. Smart Nano Mater. 12 (4) (2021) 491–510.
[38] M.A. Wagner, F. Schwarz, N. Huber, L. Geistlich, H. Galinski, R. Spolenak, Deformation-induced topological transitions in mechanical metamaterials and their application to tunable non-linear stiffening, Mater. Des. 221 (2022) 110918.
[39] O. Skarsetz, V. Slesarenko, A. Walther, Programmable auxeticity in hydrogel metamaterials via shape-morphing unit cells, Adv. Sci. 9 (23) (2022) 2201867.
[40] M. Lei, W. Hong, Z. Zhao, C. Hamel, M. Chen, H. Lu, H.J. Qi, 3d printing of auxetic metamaterials with digitally reprogrammable shape, ACS Appl. Mater. Interfaces 11 (25) (2019) 22768–22776.
[41] Z. Wang, Z. Wang, Y. Zheng, Q. He, Y. Wang, S. Cai, Three-dimensional printing of functionally graded liquid crystal elastomer, Sci. Adv. 6 (39) (2020).
[42] K.K. Dudek, J.A.I. Martínez, G. Ulliac, L. Hirsinger, L. Wang, V. Laude, M. Kadic, Micro-scale mechanical metamaterial with a controllable transition in the Poisson's ratio and band gap formation, Adv. Mater. 35 (20) (2023).
[43] K.K. Dudek, R. Gatt, M.R. Dudek, J.N. Grima, Negative and positive stiffness in auxetic magneto-mechanical metamaterials, Proc. R. Soc. A, Math. Phys. Eng. Sci. 474 (2215) (2018) 20180003.
[44] T. Chen, M. Pauly, P.M. Reis, A reprogrammable mechanical metamaterial with stable memory, Nature 589 (7842) (2021) 386–390.
[45] A. Walther, Viewpoint: from responsive to adaptive and interactive materials and materials systems: a roadmap, Adv. Mater. 32 (20) (2019) 1905111.
[46] G. Fusi, D.D. Giudice, O. Skarsetz, S.D. Stefano, A. Walther, Autonomous soft robots empowered by chemical reaction networks, Adv. Mater. 35 (7) (2022) 2209870.
[47] M.C. Huber, U. Jonas, S.M. Schiller, An autonomous chemically fueled artificial protein muscle, Adv. Intell. Syst. 4 (4) (2022) 2100189.
[48] M.F. Berwind, A. Kamas, C. Eberl, A hierarchical programmable mechanical metamaterial unit cell showing metastable shape memory, Adv. Eng. Mater. 20 (11) (2018).
[49] J. Li, V. Slesarenko, S. Rudykh, Auxetic multiphase soft composite material design through instabilities with application for acoustic metamaterials, Soft Matter 14 (30) (2018) 6171–6180.
[50] J. Shim, S. Shan, A. Košmrlj, S.H. Kang, E.R. Chen, J.C. Weaver, K. Bertoldi, Harnessing instabilities for design of soft reconfigurable auxetic/chiral materials, Soft Matter 9 (34) (2013) 8198.
[51] S. Kamrava, D. Mousanezhad, H. Ebrahimi, R. Ghosh, A. Vaziri, Origami-based cellular metamaterial with auxetic, bistable, and self-locking properties, Sci. Rep. 7 (1) (2017).
[52] F. Wenz, I. Schmidt, A. Leichner, T. Lichti, S. Baumann, H. Andrae, C. Eberl, Designing shape morphing behavior through local programming of mechanical metamaterials, Adv. Mater. 33 (37) (2021) 2008617.
[53] A. Farzaneh, N. Pawar, C.M. Portela, J.B. Hopkins, Sequential metamaterials with alternating Poisson's ratios, Nat. Commun. 13 (1) (2022).
[54] T.-C. Lim, Metamaterials with Poisson's ratio sign toggling by means of microstructural duality, SN Appl. Sci. 1 (2) (2019).
[55] C.E. Helou, B. Grossmann, C.E. Tabor, P.R. Buskohl, R.L. Harne, Mechanical integrated circuit materials, Nature 608 (7924) (2022) 699–703.
[56] H. Yasuda, P.R. Buskohl, A. Gillman, T.D. Murphey, S. Stepney, R.A. Vaia, J.R. Raney, Mechanical computing, Nature 598 (7879) (2021) 39–48.
[57] T. Reppel, K. Weinberg, Experimental determination of elastic and rupture properties of printed ninjaflex, Tech. Mech. 38 (1) (2018).
[58] C.W. Smith, R.J. Wootton, K.E. Evans, Interpretation of experimental data for Poisson's ratio of highly nonlinear materials, Exp. Mech. 39 (4) (1999) 356–362.